Published in final edited form as:
Glia. 2009 December ; 57(16): 1706–1715. doi:10.1002/glia.20882.

HETEROGENEITY OF KIR4.1 CHANNEL EXPRESSION IN GLIA REVEALED BY MOUSE TRANSGENESIS

Xiaofang Tang, **Kenichiro Taniguchi**, and **Paulo Kofuji**
Department of Neuroscience, University of Minnesota, Minneapolis, MN 55455, USA

Abstract

The weakly inwardly rectifying K^+ channel Kir4.1 is found in many glial cells including astrocytes. However, questions remain regarding the relative contribution of Kir4.1 to the resting K^+ conductance of mature astrocytes *in situ*. We employed a bacterial artificial chromosome (BAC) transgenic approach in mice to visualize Kir4.1 expression *in vivo*. These mice (Kir4.1-EGFP) express Enhanced Green Fluorescent Protein (EGFP) under the transcriptional control of the Kir4.1 promoter. The brains of adult Kir4.1-EGFP transgenic mice showed coexpression of EGFP and Kir4.1 in astrocytes. In addition, weaker expression of EGFP was detected in NG2+ glial cells when compared to EGFP expression in GFAP+ glial cells. Whole-cell voltage clamp recordings of EGFP+ glial cells in the CA1 area of the adult mouse hippocampus indicated astrocytes displaying properties consistent with both the “passive” and “complex” subpopulations. EGFP+ cells with bright fluorescence had the linear current-voltage (*I-V*) relationships and extensive gap junctional coupling characteristic of passive astrocytes. However EGFP+ glia with weaker fluorescence displayed properties associated with complex astrocytes including non-linear *I-V* relationships and lack of intercellular gap junctional coupling. Pharmacological blockade of inward currents implied that Kir4.1 channels constitute the dominant resting K^+ conductance in both glial cell types and are more highly expressed in passive astrocytes. These results suggest differential expression of Kir4.1 in glia and that this channel likely underlies the resting K^+ conductance in passive and complex astrocytes.

Keywords

Passive astrocytes; complex astrocytes; GFAP; NG2; potassium siphoning; potassium channel

INTRODUCTION

Astrocytes in the adult hippocampus can be functionally segregated into at least two major classes, one termed “passive” and the other “complex.” Passive astrocytes are characterized by their large resting membrane K^+ conductance and ohmic *I-V* relationships and express glial fibrillary acidic protein (GFAP) and the glutamate transporter GLAST (Matthias et al. 2003; Steinhauser et al. 1992; Zhou et al. 2006). Complex astrocytes, however, have a smaller resting K^+ conductance and non-linear *I-V* relationships, express the ionotropic glutamate receptor AMPA, and a subpopulation of complex astrocytes is immunoreactive to the chondroitin sulfate proteoglycan NG2 (Matthias et al. 2003; Schools et al. 2003; Zhou et al. 2006). These identified differences between complex and passive astroctyes imply that passive astrocytes are more suitable than complex astrocytes to perform a “spatial K^+

Address for correspondence: Paulo Kofuji, Department of Neuroscience, University of Minnesota, 6-145 Jackson Hall, 321 Church St SE, Minneapolis, MN 55455, Phone: 612-625-6457, FAX: 612-626-5009, kofuj001@umn.edu.

buffering" function because the plasma membrane of these cells is highly conductive to K^+ and these cells form large functional syncytiums (Wallraff et al. 2004).

Several immunocytochemical and transcript analysis studies have demonstrated the expression of Kir4.1 channels in diverse glial types (Kofuji and Newman 2004; Olsen and Sontheimer 2008). In addition, evidence supporting the functional role of Kir4.1 channels in glia was obtained in studies using a mouse line with targeted disruption of the Kir4.1 gene (Kofuji et al. 2000). In these mice, the membrane potential is highly depolarized and inward K^+ currents are diminished in retinal Muller cells (Kofuji et al. 2000), cultured spinal oligodendrocytes (Neusch et al. 2001), and brain stem astrocytes (Neusch et al. 2006). However, questions remain regarding the relative contribution of Kir4.1 channels to the resting K^+ conductance of complex and passive astrocytes in mature hippocampus. Evidence against a central role of Kir4.1 in the resting K^+ conductance of passive astrocytes includes the lack (or small effect) of Kir channel blockers on the evoked inward currents of passive astrocytes (D'Ambrosio et al. 1998; Djukic et al. 2007) and the large resting conductance of the passive astrocytes in a conditional Kir4.1 knockout mouse line (Djukic et al. 2007). Furthermore, other "leak" K^+ channels have been detected in astrocytes, raising the possibility of their contribution to the membrane K^+ conductance of the astrocytic membrane as well (Gnatenco et al. 2002; Kindler et al. 2000).

In this study, we make use of a novel BAC transgenic mouse line in which EGFP is under the transcriptional control of the Kir4.1 promoter to study the functional properties of mature glia in the CA1 area of hippocampus. We found that two cell types, identified by their differential EGFP expression, have the electrophysiological properties previously described in complex and passive astrocytes. These results support the notion that Kir4.1 underlies the conductance of distinct glial subpopulations possessing unique functional and morphological properties.

MATERIALS AND METHODS

Generation of Kir4.1-EGFP BAC transgenic mouse line

BAC recombination was performed as described previously (Schmidt et al. 2008). The BAC clone RP23-157J4, containing ~132 kb and ~52 kb of DNA flanking the 5′ and 3′ ends of the Kir4.1 gene locus (KCNJ10), respectively, was obtained from the BAC resource at Children's Hospital Oakland Research Institute and chosen to insert a cassette containing an EGFP-PolyA (Clontech, Mountain View, CA) and a Kanamycin/Neomycin resistance gene flanked by two FRT sites.

Antibodies

Primary antibodies used in this study are listed in Table 1. For secondary antibodies in immunocytochemistry, we used AlexaFluor antibodies (Invitrogen, Carlsbad, CA) produced in goat, including anti-rabbit488 and 594; anti-mouse 488, 594 and 647. For detection on Western blotting, we used peroxidase-conjugatedanti-mouse (working concentration 1:30,000) or anti-rabbit (1:20,000) (Jackson ImmunoResearch Laboratories, Inc., West Grove, PA).

Immunocytochemistry

Immunocytochemistry and image analyzes were performed as described previously (Schmidt et al. 2008).

Western Blotting

Mouse brains (P14 to P21) were used for Western blots using procedures as described previously (Connors et al. 2004).

Electrophysiology

For whole-cell patch-clamp recordings we used P21 to P30 mice. 250- to 350-μm coronal hippocampal brain slices were sectioned in ice-cold, oxygenated (95% O_2-5% CO_2) cutting solution (in mM): 220 sucrose, 26 $NaHCO_3$, 3 KCl, 5 $MgCl_2$, 1.25 NaH_2PO_4, 1.0 $CaCl_2$, 10 glucose (pH 7.2). These slices were initially incubated for 20 min at ~34° C and allowed to cool to room temperature in artificial cerebral spinal fluid (aCSF) (in mM): 130 NaCl, 26 $NaHCO_3$, 3 KCl, 2 $MgCl_2$, 1.25 NaH_2PO_4, 2 $CaCl_2$, 10 glucose (pH 7.2). Slices were transferred to a recording chamber mounted on the stage of an upright microscope (E600 FN, Nikon, Tokyo, Japan) equipped with differential interference contrast optics and epifluorescence, which was used to visualize EGFP-expressing cells in the brain slice. Whole-cell recordings were made at room temperature from the soma of fluorescent glia in the CA1 area of hippocampus using a Multiclamp 700A amplifier (Axon Instruments, Union City, CA) with fire-polished borosilicate pipettes (3 – 7 MΩ, Sutter Instruments, Novato, CA) filled with (in mM): 125 KGluconate, 2 $CaCl_2$, 2 $MgCl_2$, 10 EGTA, 10 HEPES, 0.5 NaGTP, and 2 Na_2ATP, pH with KOH (pH 7.2). Bath solution consisted of aCSF solution as described above. All traces were sampled at 5 – 10 kHz and low-pass filtered at 2 kHz. Liquid junction potentials were not corrected. Measurements of cell resistance were derived from currents evoked by stepping the cell potential to a 10 mV hyperpolarized value for 20 ms from a holding potential of −60 mV. When the experiment was carried out using a pipette solution containing 0.5% biocytin (Sigma, Saint Louis, MO), patch pipettes were carefully detached from the recorded cells, and the slices were then fixed with PFA overnight at 4°C. Biocytin was visualized with rhodamine conjugated streptavidin (Jackson Immunoresearch Laboratories, West Grove, PA).

Statistics

Numerical values are given as mean ± SE. All comparisons across conditions for the same datasets were made by using Student's t-tests.

RESULTS

Generation and validation of Kir4.1-EGFP BAC transgenic mice

A BAC containing the Kir4.1 gene (KCNJ10) and 132 kb of 5′ sequences and 52 Kb of 3′ sequences was used for generation of transgenic mice (Figure 1A). In this BAC, the coding sequence of the Kir4.1 channel, which is contained in a single exon, was replaced with sequences encoding EGFP by BAC recombination (Yang et al. 1997). Four independent founder lines were generated with similar patterns of EGFP expression in brain and retina. Widespread intrinsic EGFP fluorescence was observed in brain tissue sections from adult mice (Figure 1B) with numerous brightly fluorescent cells (Figures 1C-H). In the hippocampus, large pyramidal neuronal cells lacked EGFP signal while smaller stellate-shaped cells were brightly fluorescent, consistent with glial expression of EGFP (Figures 1C-D). A similar pattern of fluorescence was also detected in cortex (Figure 1E). In the cerebellum, the Bergman glia in the molecular layer and astrocytes in the granule layer were strongly labeled (Figures 1F-G). Double staining with anti-NeuN to label neurons and anti-EGFP antibodies in the hippocampus and cortex showed that neurons lacked EGFP expression (Figures 2A-C), further supporting glial EGFP expression.

It was possible that the extra copies of Kir4.1 promoter regions present on the Kir4.1-EGFP transgene would interfere with expression of endogenous Kir4.1 channels. To address this

possibility, we performed Western Blots using brain lysates from either wild type or Kir4.1-EGFP littermates to compare levels of Kir4.1 protein. As can be seen in Figures 1I-J, comparable levels of Kir4.1 expression were detected in the brains of wild type and Kir4.1-EGFP mice. These results indicate that endogenous expression of Kir4.1 channels was not perturbed in the Kir4.1-EGFP mouse line.

To validate this mouse line as a reporter of Kir4.1 expression, it was also essential to demonstrate the correlated expression of EGFP and Kir4.1. To test this, we used immunocytochemistry in hippocampal and cortical slices from Kir4.1-EGFP mice to localize expression of EGFP and Kir4.1 (Figures 2D-I). When cells from CA1 area of hippocampus (n=849) and cortex (n= 337) were counted, coexpression of EGFP and Kir4.1 was seen in about 97% of cells (supplementary material S1). EGFP expression concentrated in the soma as expected for the expression of a cytoplasmic protein (Figures 2D, G) and with expression being more diffuse, though somewhat localized to the plasma membrane (Figures 2E, H). Such co-expression of Kir4.1 channels and EGFP was also seen in other brain regions such as olfactory bulb and cerebellum (result not shown). Overall these results indicate the fidelity of EGFP as a reporter of Kir4.1 expression in the Kir4.1-EGFP mouse line.

Differential expression of Kir4.1 channels in glia

We next asked whether Kir4.1 channels are expressed in various glial subpopulations, i.e. the GFAP and NG2-expressing glia. We performed triple labeling and confocal imaging for NG2, GFAP and EGFP in cortical and hippocampal slices (Figures 3A-H). GFAP or NG2 immunoreactivity was found in cells with either round or irregular somas. GFAP immunostaining revealed the main radial processes as expected for a cytoskeletal protein while NG2 immunostaining demarcated processes and the cells somas (Figures 3A-H). Comparisons of relative fluorescence levels revealed that intense EGFP signals were found preferentially in astrocytes that were also GFAP+ (Figures 3A-H). NG2+ cells, on the other hand, displayed weaker expression of EGFP although clearly above background fluorescence levels (Figures 3A-H). Fluorescence signal for EGFP was significantly higher in GFAP+ glia than in NG2+ glia ($P < 0.005$, Student's t-test) and in general the GFAP+ glia outnumbered NG2+ glia in the CA1 area of the hippocampus (Figure 3I).

EGFP+ glia in hippocampus have either "passive" or "complex" properties

The heterogeneous expression of EGFP in GFAP+ and NG2+ cells implies the differential expression of Kir4.1 in these two populations of glia, which led us to examine their physiological properties in more detail. Whole-cell patch clamp recordings from weakly fluorescent cells (Figure 4A-B) in the CA1 area of the hippocampus revealed that these cells displayed the hyperpolarized membrane potentials (−78.9 ± 0.4 mV, n= 62) and relative high resistances (121.9 ± 9.2 MΩ, n= 62). Voltage steps from (−160 to +30 mV revealed multiple points of rectification with both inwardly and outwardly rectifying currents (Figure 4B). This electrophysiological profile is characteristic of complex, or variably rectifying, astrocytes (Zhou et al. 2006). This class of glial cell is also known to lack intercellular electrical coupling (Schools et al. 2006; Wallraff et al. 2004). We verified this lack of coupling in weakly fluorescent cells by injection, via patch pipette, of biocytin, which easily passes through gap junctions (Vaney 1991). Confocal microscopy of biocytin-filled cells confirmed a lack of biocytin diffusion to neighboring cells within hippocampal slices (Figure 5E and supplementary material S2A). Moreover, NG2 immunoreactivity co-localized with single biocytin-filled cells (n=6) (supplementary material S3A). Overall these findings indicate a defined subpopulation of glial cells that can be identified by their weak EGFP fluorescence and possess the functional and morphological features previously described for complex astrocytes in mature hippocampus (Zhou et al. 2006).

We next sought to identify the functional properties of brightly fluorescent cells and to compare them to those identified in weakly fluorescent cells. Whole-cell voltage clamp recordings from cells with higher levels of EGFP expression revealed hyperpolarized membrane potentials ((−78.5 ±0.3 mV, n= 89) similar to those measured in weakly fluorescent cells. However the input resistances of brightly fluorescent were markedly lower (17.9 ± 0.4 MΩ, n= 89) than those measured in weakly fluorescent cells ($P < 0.0001$, Student's t-test). Voltage steps from (−160 mV to + 30 mV elicited essentially time and voltage-independent currents resulting in linear whole-cell *I-V* relationships (Figure 4C), in contrast to the rectifying *I-V* profile seen in weakly fluorescent cells. Moreover, we observed a high degree of intercellular electrical coupling among brightly fluorescent cells as revealed by the extensive spread of biocytin from the recorded brightly fluorescent astrocyte to neighboring cells. Confocal microscopy of biocytin-filled, brightly fluorescent cells, showed biocytin staining of numerous neighboring cells that were also EGFP+ (supplementary material S2B). This high degree of intercellular coupling (40 ± 3 coupled cells/slice, n=22) was never observed upon dye-filling of weakly fluorescent cells (supplementary material S2C). Finally, staining of biocytin-filled, brightly fluorescent cells with either anti-GFAP or NG2 antibodies revealed that these cells displayed immunoreactivity towards GFAP but not NG2 (supplementary material S3B,C). Thus, glial cells with high levels of EGFP expression have the hallmark properties of so called passive astrocytes (Matthias et al. 2003; Schools et al. 2006; Wallraff et al. 2004). Overall, these results suggest that heterogeneity in EGFP content in glial cells of Kir4.1-EGFP distinguishes distinct subpopulations of astrocytes.

One method used to assess the contribution of Kir channels to the basal conductance of cells is to verify whether inward currents are susceptible to blockade by pharmacological agents such as cesium and barium (Doupnik et al. 1995). In addition, the tricyclic anti-depressant desipramine reversibly inhibits Kir4.1 currents in a concentration-dependent manner, while only marginally affecting Kir2.1 currents in heterologous expression systems (Su et al. 2007). We assessed the effect of these Kir channel blockers in both weakly and brightly fluorescent cells. In cells with low levels of EGFP expression, bath application of cesium (1 mM) resulted in the characteristic voltage-dependent blockade of inward currents (Figure 5A) without significantly affecting outward currents. Barium (100 μM), in contrast, reduced both inward and outward currents (Figure 5B) and induced depolarization of the membrane potential (9.9 ± 1.5 mV shift, n=6) (Figure 5B). Similar results were also observed using desipramine (100 μM) (Figure 5C).

Surprisingly, cesium and barium applied in the bath inhibited just a fraction of evoked currents in brightly fluorescent cells (Figure 6A and data not shown). Because filling of brightly fluorescent cells resulted in diffusion of the tracer biocytin to neighboring astrocytes (Figure 6E), we reasoned that the lack of current blockade by cesium and barium could be caused by inaccessibility of the drugs to coupled cells deeper in the slice. To test this, we recorded from brightly fluorescent cells in slices which had been pretreated with the gap junctional blocker meclofenamic acid (MFA), a reversible connexin 43 blocker (Harks et al. 2001). Pretreatment of slices with MFA for 30–40 min did not alter the "passive" type current profile of brightly fluorescent cells (Supplementary material S4B) but it was effective in preventing the diffusion of biocytin to neighboring cells (Supplementary material S4A, C). Under these conditions, both cesium and barium blocked the large evoked inward currents in brightly fluorescent cells (Figure 6B–D).

To test the notion that the heterogeneity of fluorescence between glial cells reflects heterogeneity of Kir4.1 promoter activity and thus heterogeneity of Kir4.1 expression, we compared barium-sensitive currents following MFA treatment in passive astrocytes to those measured in complex astrocytes. If there is higher Kir4.1 expression in those cells with brighter EGFP signals, then we would expect larger barium-sensitive currents in brighter

fluorescent cells. Indeed, barium-sensitive currents were significantly larger in passive astrocytes (brightly fluorescent cells) treated with MFA ((−1962.1 ± 177.6 pA at (−140 mV, n=11) than in complex astrocytes (weakly fluorescent cells) ((−674.7 ± 83.1pA at (−140 mV, n=8)(data not shown)($P < 0.05$, Student's t-test).

DISCUSSION

Collectively our results indicate the significant and yet differential expression of the Kir4.1 subunit in functionally identified complex and passive astrocytes in mature mouse hippocampus. While there have been reports of Kir4.1 transcript or protein in glial cells of the hippocampus (Hibino et al. 2004; Poopalasundaram et al. 2000; Schroder et al. 2002), it has remained unclear whether this channel subunit contributes appreciably to the resting K^+ conductance of complex and passive astrocytes. For example, in a study by D'Ambrosio et al. (1998), passive astrocytes (named linear type in their study) showed a virtual absence of cesium-sensitive currents. Likewise, passive astrocytes recorded from wild type mouse hippocampus have been shown to have only small barium-sensitive currents (Djukic et al. 2007). These results would be inconsistent with a significant role of Kir4.1 channels to the resting K^+ conductance of passive astrocytes.

We took a BAC transgenic approach to provide further insights into the patterns of Kir4.1 expression in mouse brain. Our expectation was that EGFP under the transcriptional control of Kir4.1 promoter would reveal its differential expression among cellular subtypes. Upon examination of fluorescence in the Kir4.1-EGFP mouse brain, we did in fact observe heterogeneity of EGFP expression, with weakly and brightly fluorescent cells being present in both grey and white matter. We chose to investigate these cell types in the CA1 area of the hippocampus given the extensive functional and anatomical characterization of astrocytes in this brain region (Matthias et al. 2003; Schools et al. 2006; Wallraff et al. 2004; Zhou et al. 2006). We chose to perform these studies in adult mice (i.e. older than P21) as the degree of electrophysiological diversity is minimized at later developmental stages (Zhou et al. 2006). Whole-cell electrophysiological recordings and immunocytochemical studies of weakly fluorescent cells revealed many of the properties associated with complex astrocytes such as non-linear *I-V* relationships, expression of NG2, and lack of gap junctional coupling with neighboring cells (Schools et al. 2006; Zhou and Kimelberg 2000). These results corroborate data recently obtained in a Kir4.1 conditional knockout line by Djukic et al. (2007), in which the complex astrocytes from the mutant mouse were highly affected, displaying depolarized membrane potentials and high input resistances. These results also support single cell RT-PCR analyses in which complex astrocytes expressed transcripts for Kir4.1, though less frequently than Kir2.1, Kir2.2 and Kir2.3 (Schroder et al. 2002). The almost complete blockade of inward currents with desipramine in our study favors the hypothesis that Kir4.1 is the principal functional subunit mediating the resting K^+ conductance in complex cells. At the present moment the role of complex astrocytes in the mature brain remains unclear in particular in the grey matter. The lack of intercellular coupling as evidenced by the confinement of biocytin to the recorded cell makes unlikely that these weakly fluorescent, complex astrocytes have a prominent role in spatial potassium buffering.

In contrast, recordings from brightly fluorescent cells showed many features commonly associated with passive astrocytes. Interestingly, substantial blockade of inward currents by Kir channel blockers such as barium and cesium was revealed only following the treatment of hippocampal slices with the gap junctional blocker MFA. Presumably, the extensive electrical coupling among passive astrocytes in untreated slices prevented the assessment of Kir4.1 channel expression using the pharmacological blockers. This may explain why in the study by Djukic et al. (2007) barium elicited only modest effects on inward currents of

passive astrocytes. This formation of functional syncytiums and the large K^+ conductance of brightly fluorescent cells could provide the optimal cellular substrate for the spatial redistribution of K^+ in the extracellular environment. Indeed several studies upon knockdown or knockout of Kir4.1 have indicated some impairment in the regulation of $[K^+]_o$ in brain (Olsen and Sontheimer 2008). One potential limitation of our study is that we performed all electrophysiological recordings in relatively young mice (P21–30) when there is still rapid accumulation of myelin basic protein in mouse brain (Barbarese et al, 1978). It is conceivable that the observed functional heterogeneity for Kir4.1 expression to diminish in more mature mice.

In summary our results indicate a surprising heterogeneity of Kir4.1 promoter activity in mature hippocampus revealing its differential expression in glial subtypes. In both complex and passive astrocytes, Kir4.1 seems to constitute the dominant K^+ conductance in the plasma membrane. The expected central role of Kir4.1 channels in regulation of $[K^+]_o$ in the CNS and their restricted glial expression make such channels attractive targets for treatments of disorders related to excessive neuronal excitability.

Supplementary Material

Refer to Web version on PubMed Central for supplementary material.

Acknowledgments

This work was supported by National Institutes of Health grants EY12949 and EY011374. We would like to thank the immense help by Jill O'Moore on the transgenic mice generation and Tiffany M. Schmidt for the comments on the manuscript.

References

Barbarese E, Carson JH, Braun PE. Accumulation of four myelin basic proteins in mouse during development. J Neurochem. 1978:779–782. [PubMed: 81270]

Connors NC, Adams ME, Froehner SC, Kofuji P. The potassium channel Kir4.1 associates with the dystrophin glycoprotein complex via alpha-syntrophin in glia. J Biol Chem. 2004; 279:28387–92. [PubMed: 15102837]

D'Ambrosio R, Wenzel J, Schwartzkroin P, McKhann GI, Janigro D. Functional specialization and topographic segregation of hippocampal astrocytes. J Neurosci. 1998; 18:4425–38. [PubMed: 9614220]

Djukic B, Casper KB, Philpot BD, Chin LS, McCarthy KD. Conditional knock-out of Kir4.1 leads to glial membrane depolarization, inhibition of potassium and glutamate uptake, and enhanced short-term synaptic potentiation. J Neurosci. 2007; 27:11354–65. [PubMed: 17942730]

Doupnik CA, Davidson N, Lester HA. The inward rectifier potassium channel family. Curr Opin Neurobiol. 1995; 5:268–77. [PubMed: 7580148]

Gnatenco C, Han J, Snyder AK, Kim D. Functional expression of TREK-2 K+ channel in cultured rat brain astrocytes. Brain Res. 2002; 931:56–67. [PubMed: 11897089]

Harks EG, de Roos AD, Peters PH, de Haan LH, Brouwer A, Ypey DL, van Zoelen EJ, Theuvenet AP. Fenamates: a novel class of reversible gap junction blockers. J Pharmacol Exp Ther. 2001; 298:1033–41. [PubMed: 11504800]

Hibino H, Fujita A, Iwai K, Yamada M, Kurachi Y. Differential assembly of inwardly rectifying K+ channel subunits, Kir4.1 and Kir5.1, in brain astrocytes. J Biol Chem. 2004; 279:44065–73. [PubMed: 15310750]

Kindler CH, Pietruck C, Yost CS, Sampson ER, Gray AT. Localization of the tandem pore domain K+ channel TASK-1 in the rat central nervous system. Brain Res Mol Brain Res. 2000; 80:99–108. [PubMed: 11039733]

Kofuji P, Ceelen P, Zahs KR, Surbeck LW, Lester HA, Newman EA. Genetic inactivation of an inwardly rectifying potassium channel (Kir4.1 subunit) in mice: phenotypic impact in retina. J Neurosci. 2000; 20:5733–40. [PubMed: 10908613]

Kofuji P, Newman EA. Potassium buffering in the central nervous system. Neuroscience. 2004; 129:1045–56. [PubMed: 15561419]

Matthias K, Kirchhoff F, Seifert G, Huttmann K, Matyash M, Kettenmann H, Steinhauser C. Segregated expression of AMPA-type glutamate receptors and glutamate transporters defines distinct astrocyte populations in the mouse hippocampus. J Neurosci. 2003; 23:1750–8. [PubMed: 12629179]

Neusch C, Papadopoulos N, Muller M, Maletzki I, Winter SM, Hirrlinger J, Handschuh M, Bahr M, Richter DW, Kirchhoff F, et al. Lack of the Kir4.1 channel subunit abolishes K+ buffering properties of astrocytes in the ventral respiratory group: impact on extracellular K+ regulation. J Neurophysiol. 2006; 95:1843–52. [PubMed: 16306174]

Neusch C, Rozengurt N, Jacobs RE, Lester HA, Kofuji P. Kir4.1 potassium channel subunit is crucial for oligodendrocyte development and in vivo myelination. J Neurosci. 2001; 21:5429–38. [PubMed: 11466414]

Olsen M, Sontheimer H. Functional Implications for Kir4.1 Channels in Glial Biology: From K+ Buffering to Cell Differentiation. J Neurochem. 2008; 107:589–601. [PubMed: 18691387]

Poopalasundaram S, Knott C, Shamotienko OG, Foran PG, Dolly JO, Ghiani CA, Gallo V, Wilkin GP. Glial heterogeneity in expression of the inwardly rectifying K(+) channel, Kir4.1, in adult rat CNS. Glia. 2000; 30:362–72. [PubMed: 10797616]

Schmidt TM, Taniguchi K, Kofuji P. Intrinsic and extrinsic light responses in melanopsin-expressing ganglion cells during mouse development. J Neurophysiol. 2008; 100:371–84. [PubMed: 18480363]

Schools GP, Zhou M, Kimelberg HK. Electrophysiologically “complex” glial cells freshly isolated from the hippocampus are immunopositive for the chondroitin sulfate proteoglycan NG2. J Neurosci Res. 2003; 73:765–77. [PubMed: 12949902]

Schools GP, Zhou M, Kimelberg HK. Development of gap junctions in hippocampal astrocytes: evidence that whole cell electrophysiological phenotype is an intrinsic property of the individual cell. J Neurophysiol. 2006; 96:1383–92. [PubMed: 16775204]

Schroder W, Seifert G, Huttmann K, Hinterkeuser S, Steinhauser C. AMPA receptor-mediated modulation of inward rectifier K+ channels in astrocytes of mouse hippocampus. Mol Cell Neurosci. 2002; 19:447–58. [PubMed: 11906215]

Steinhauser C, Berger T, Frotscher M, Kettenmann H. Heterogeneity in the Membrane Current Pattern of Identified Glial Cells in the Hippocampal Slice. Eur J Neurosci. 1992; 4:472–484. [PubMed: 12106333]

Su S, Ohno Y, Lossin C, Hibino H, Inanobe A, Kurachi Y. Inhibition of astroglial inwardly rectifying Kir4.1 channels by a tricyclic antidepressant, nortriptyline. J Pharmacol Exp Ther. 2007; 320:573–80. [PubMed: 17071817]

Vaney DI. Many diverse types of retinal neurons show tracer coupling when injected with biocytin or Neurobiotin. Neurosci Lett. 1991; 125:187–90. [PubMed: 1715532]

Wallraff A, Odermatt B, Willecke K, Steinhauser C. Distinct types of astroglial cells in the hippocampus differ in gap junction coupling. Glia. 2004; 48:36–43. [PubMed: 15326613]

Yang XW, Model P, Heintz N. Homologous recombination based modification in Escherichia coli and germline transmission in transgenic mice of a bacterial artificial chromosome. Nat Biotechnol. 1997; 15:859–65. [PubMed: 9306400]

Zhou M, Kimelberg HK. Freshly isolated astrocytes from rat hippocampus show two distinct current patterns and different [K(+)](o) uptake capabilities. J Neurophysiol. 2000; 84:2746–57. [PubMed: 11110805]

Zhou M, Schools GP, Kimelberg HK. Development of GLAST(+) astrocytes and NG2(+) glia in rat hippocampus CA1: mature astrocytes are electrophysiologically passive. J Neurophysiol. 2006; 95:134–43. [PubMed: 16093329]

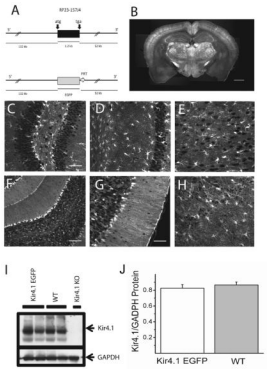

Figure 1. Generation and initial characterization of Kir4.1-EGFP mouse line

(A) Schematic representation of the transgene Kir4.1-EGFP. The 185 kb mouse genomic bacterial artificial chromosome (BAC) clone RP23 – 157J4 containing the entire transcriptional unit of Kir4.1 together with 132 kb upstream and 52 kb downstream was engineered to harbor EGFP coding sequences followed by a polyadenylation signal (pA) into the coding region of Kir4.1 gene by homologous recombination in E. coli. **(B)** Intrinsic EGFP signal in coronal section of Kir4.1-EGFP mouse brain. **(C–H)** Intrinsic EGFP signals of Kir4.1-EGFP mouse brain in dentate gyrus of hippocampus (C), area CA1 of hippocampus (D), cortex (E), cerebellum (F-G), and olfactory bulb (H). **(I–J)** Western blot analyses of Kir4.1 channel expression in Kir4.1-EGFP and wild-type mouse brains. Arrows indicate the bands corresponding to Kir4.1 and glyceraldehyde-3-phosphate dehydrogenase (GAPDH). Kir4.1 knockout (KO) mouse brain was used as a control for the specificity of anti-Kir4.1 antibody used (I). Similar levels of Kir4.1 channel expression was verified using densitometric analyzes (n=5)(J). Scale bars: 1 mm (B), 50 μm (C,D,E,G,H) 100 μm (F).

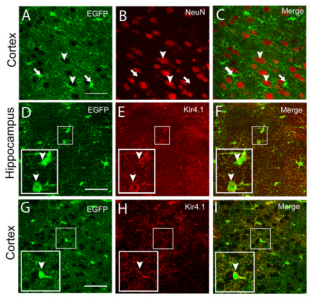

Figure 2. EGFP is not expressed in neurons and co-localizes with Kir4.1 in brain

(A–C) Immunostaining for EGFP and NeuN in the Kir4.1-EGFP cortex. Notice the expression of EGFP (arrows) in small cell bodies and lack of expression in NeuN+ cells (arrowheads). **(D–I)** Immunostaining for EGFP and Kir4.1 in area CA1 of the hippocampus (D–F) and cortex (G–I). Small squares are shown enlarged in insets in the lower left corners of each panel. Arrowheads indicate EGFP-positive cells that clearly show Kir4.1 expression in the soma. Scale bars: 50 μm (A,D,G).

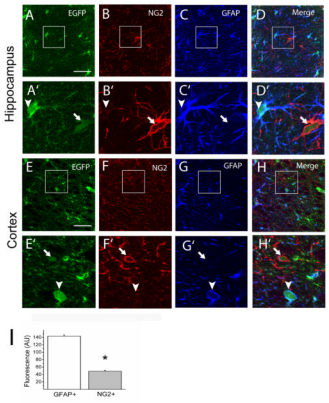

Figure 3. Kir4.1 is highly expressed in GFAP+ glia and weakly expressed in NG2+ glia in the gray matter of Kir4.1-EGFP mouse brain

(A–H) Triple labeling of brain sections for Enhanced green fluorescent protein (EGFP), chondroitin sulfate proteoglycan NG2 (NG2) and Glial fibrillary acidic protein (GFAP). Areas in the small squares are enlarged in corresponding lower figures. Arrowheads indicate GFAP+ cells while arrows indicate NG2+ cells. **(I)** The EGFP signal for the soma of cells identified as either GFAP+ (n = 264) or NG2+ (n = 103) was quantified and shown as fluorescence intensity in arbitrary units, * $P < 0.05$. Scale bars: 50 μm (A, E).

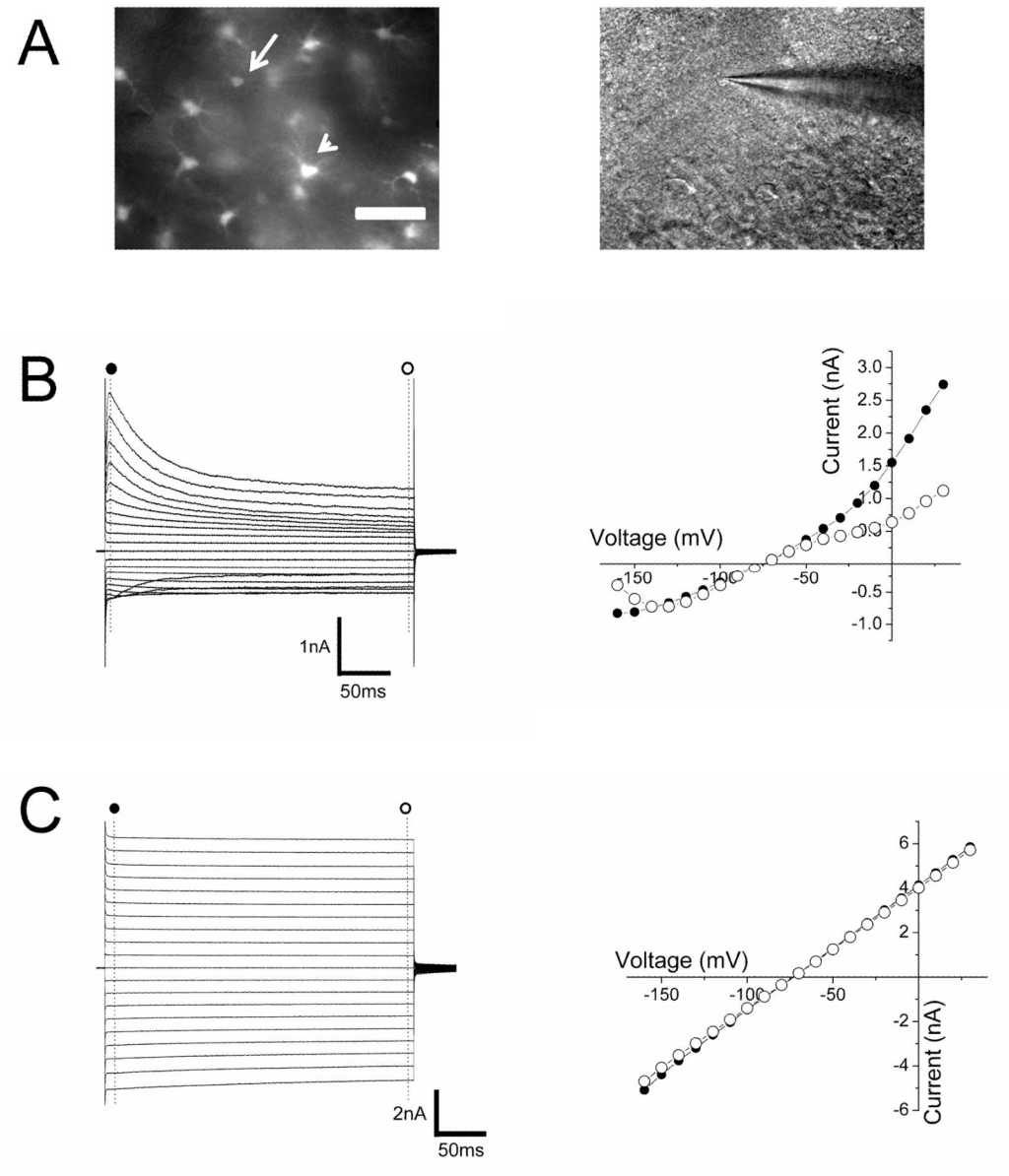

Figure 4. Weakly and brightly fluorescent glia in CA1 of hippocampus display distinct functional properties

(A) Left panel shows epifluorescence image of weakly (arrow) and brightly (arrowhead) fluorescent glia. DIC image in the right panel shows the recording pipette in the weakly fluorescent cell shown in the left panel magnification. **(B,C)** Currents elicited and *I-V* relationship upon voltage steps from −160 to +30 mV in weakly (**B**) and brightly (**C**) fluorescent cells at the beginning (●) and the end of the pulse (○). Scale bar: 50 μm (A).

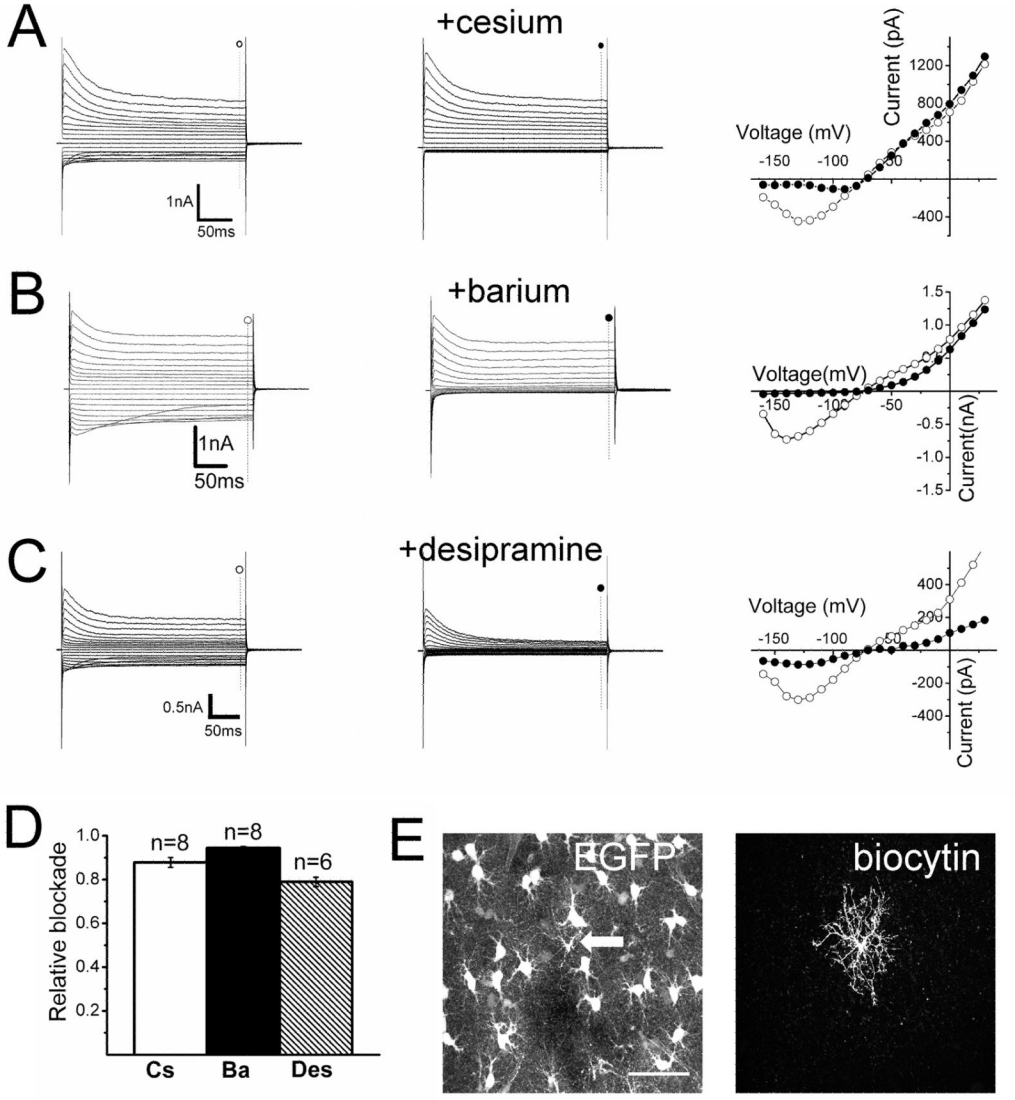

Figure 5. Pharmacological blockade of evoked currents in weakly fluorescent glia

(A–C) Current traces and *I-V* relationships in the absence (○) and presence (●) of 1 mM cesium (A), 100μM barium (B) or 100 μM desipramine (C) in the bath. (D) Summary of the relative blockade at −140 mV for cesium (Cs), barium (Ba) or desipramine (Des). (E) Confocal reconstruction of a recorded weakly fluorescent glial cell filled with biocytin (arrow). Scale bar = 50 μm.

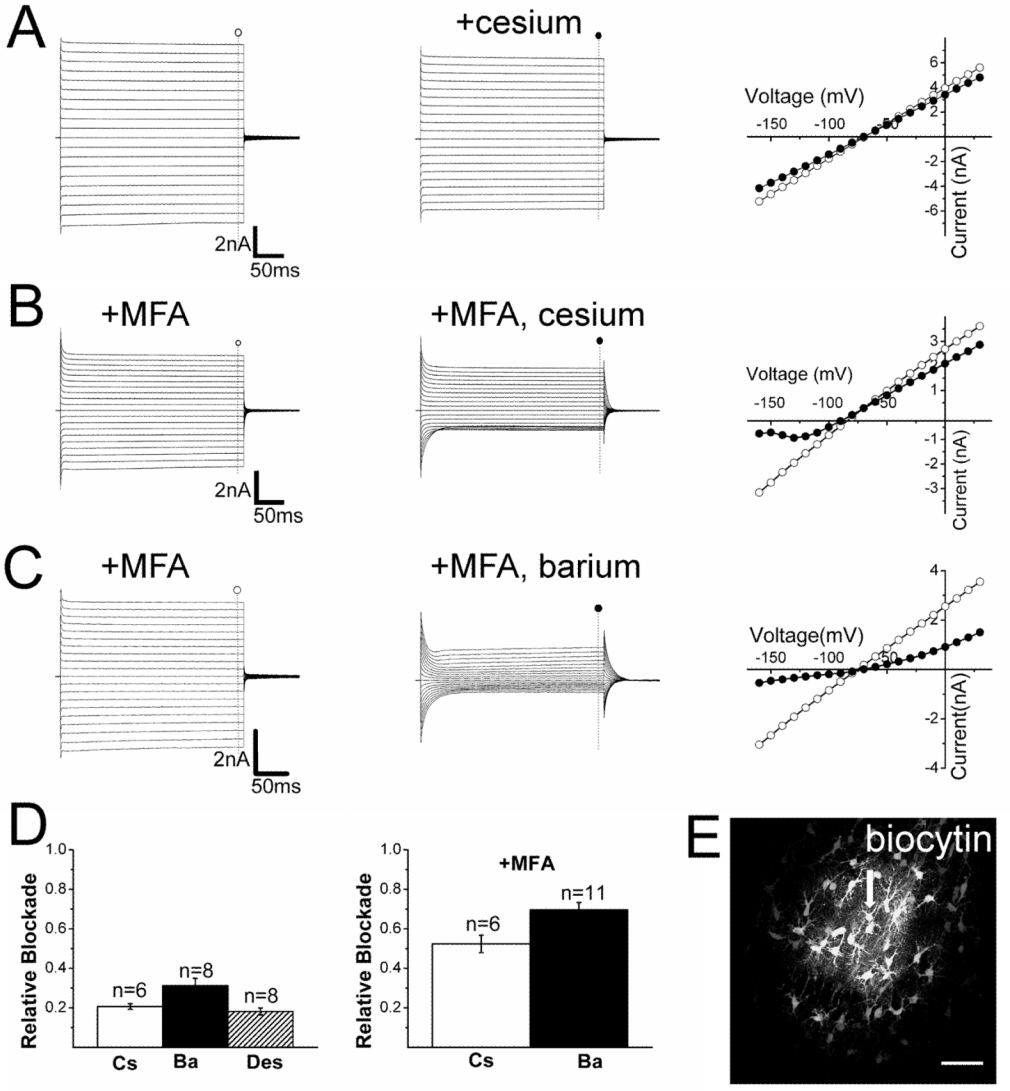

Figure 6. Pharmacological blockade of currents evoked in brightly fluorescent glia

(A) Current traces and *I-V* relationships in the absence (○) and presence (●) of 1 mM cesium. (B, C) Current traces and *I-V* relationships in the absence (○) and presence (●) of 1 mM cesium (B) or 100 μM barium (C) plus 100 μM meclofenamic acid (MFA). (D) Summary of the relative current blockade at −140 mV for cesium (Cs), barium (Ba) or desipramine (Des) in presence or absence of MFA. (E) Confocal reconstruction of a recorded brightly fluorescent cell (arrow) filled with biocytin. Notice the spread of the tracer biocytin to neighboring cells. Scale bar = 50 μm.

TABLE 1

ANTIBODY	ANTIGEN	DILUTION	PREPARATION	SPECIES	IMMUNIZING ANTIGEN	SOURCE
GFAP	Glial Fibrillary Acidic Protein	1:500	Monoclonal	Mouse	Purified GFAP from porcine spinal cord	MAB360, Millipore, Billerica, MA
rEGFP	Enhanced Green Fluorescent Protein	1:1000	Polyclonal	Rabbit	Full length recombinant GFP made in Escherichia coli.	Ab290, Abcam, Cambride, MA
mEGFP	Enhanced Green Fluorescent Protein	1:200	Monoclonal	Mouse	Full length recombinant GFP made in Escherichia coli.	A11120, Invitrogen, Carlsbad, CA
NG2	Chondroitin Sulfate Proteoglycan	1:100	Polyclonal	Rabbit	Immunoaffinity purified NG2 Chondroitin Sulfate Proteoglycan from rat	AB5320, Millipore
Kir4.1	Kir4.1 channel	1:1000	Polyclonal	Rabbit	Synthetic Peptide (KLEESLREQAEKEGSALSV R) from the carboxy-terminus of rat Kir4.1	APC-035, Alomone, Jesuralem, Israel
Kir4.1	Kir4.1 channel	1:200	Polyclonal	Rabbit	Synthetic Peptide (EKEGSALSVRISNV) from the carboxy-terminus of rat Kir4.1	Kofuji et al., 2000
NeuN	Neuron Specific protein NeuN	1:100	Monoclonal	Mouse	Purified cell nuclei from mouse brain	MAB377, Millipore, Billerica, MA
GADPH	Glyceraldehyde-3-Phosphate Dehydrogenase	1:3000	Monoclonal	Mouse	Glyceraldehyde-3-phosphate dehydrogenase from rabbit muscle	MAB374, Millipore, Billerica, MA